Dynamic Critical Response in Damped Random Spring Networks

Brian P. Tighe

Process & Energy Laboratory, Delft University of Technology, Leeghwaterstraat 44, 2628 CA Delft, The Netherlands

(Received 15 March 2012; published 17 October 2012)

The isostatic state plays a central role in organizing the response of many amorphous materials. We construct a diverging length scale in nearly isostatic spring networks that is defined both above and below isostaticity and at finite frequencies and relate the length scale to viscoelastic response. Numerical measurements verify that proximity to isostaticity controls the viscosity, shear modulus, and creep of random networks.

DOI: 10.1103/PhysRevLett.109.168303 PACS numbers: 83.60.Bc, 63.50.−x, 64.60.Ht

Random networks of springs display two distinct phases distinguished by the presence or absence of floppy modes—zero frequency motions that neither compress nor stretch springs. Floppiness is related to network structure via the mean coordination z [1,2]; networks with floppy modes reside below the isostatic coordination z_c. Many amorphous materials possess an isostatic state, including fiber networks, covalent glasses, foams, and emulsions. Hence the viscoelasticity of damped random networks, which remains poorly understood, could provide insight into a broad class of materials, including the relationship between structure and response [2–14].

One dramatic impact of floppiness on response is apparent in the compliance $J(s) = s\gamma(s)/\sigma_0$ (Fig. 1), which measures the Laplace-transformed shear strain $\gamma(s)$ accrued after a small step stress σ_0. At short times, networks creep forward with an evolving strain rate. At long times or small s, hypostatic networks below z_c flow steadily ($J \sim 1/s$), while hyperstatic networks above z_c approach constant strain ($J \sim s^0$). Thus networks with floppy modes are fluids, and those without are solids. The shifting curves in Fig. 1 indicate that elasticity and viscosity vary with proximity to z_c. Consistent with prior work on networks [5,6,11–14], these data strongly suggest that the isostatic state is a nonequilibrium critical point. We will show that the distance to isostaticity $\Delta z \equiv z - z_c$ indeed controls viscoelasticity in random spring networks, as it does in soft sphere packings [9,15].

One expects to find a diverging length scale near a critical point [16]. While hyperstatic networks are known to possess an *isostatic length* $\ell^* \sim 1/\Delta z$, it only governs quasistatic response above z_c [17–21]. The isostatic length should have a generalization $\xi_\pm(\Delta z, \omega)$ that is valid not only above z_c but also below and at finite frequency ω (or rate s). Here we demonstrate how to construct $\xi_\pm$ and show that it is the size of a finite system in which elastic storage and viscous loss balance. We also relate $\xi_\pm$ to response functions such as $J(s)$ and the complex shear modulus $G^*(\omega)$. We find their rate and frequency dependence matches those of jammed solids, biopolymer networks, and athermal suspensions [7,9,10].

Random spring networks.—Maxwell's counting argument gives the critical coordination $z_c = 2d$ for central force networks in d dimensions [1,2]. We generate networks near z_c according to the protocol of Ref. [6]. Beginning with a network with $z - z_c \sim O(1)$ derived from a disordered sphere packing, springs are randomly cut to reach a targeted z. Springs are cut only if the affected nodes retain at least $d + 1$ springs; we present numerical results for $d = 2$, though predicted scalings will turn out to be independent of d. Such "cutting with a local rule" guarantees that all springs belong to a single connected cluster and suppresses fluctuations in local coordination. This promotes mean field response; randomly cut spring networks display different critical exponents and a lower critical coordination [22].

A network's nodes are connected by springs at their rest length with stiffness k. When nodes undergo displacements $\{\vec{U}_i\}$, the elastic force from node j on node i, $\vec{f}_{ij} = k u_{ij}^{\parallel} \hat{n}_{ij}$, is along the unit vector $\hat{n}_{ij}$ pointing from i to j and proportional to the relative normal displacement $u_{ij}^{\parallel} = (\vec{U}_j - \vec{U}_i) \cdot \hat{n}$. We employ Durian's nonaffine damping force $\vec{F}^{\rm visc} = -b\dot{\vec{U}}^{\rm na} = -b(\dot{\vec{U}} - \dot{\vec{U}}^{\rm aff})$ [23]. This force opposes the difference between a node's velocity and the

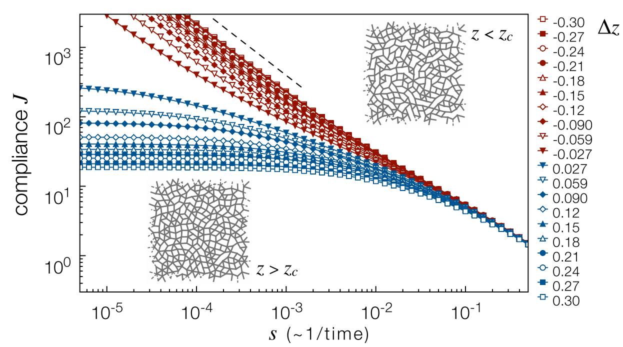

FIG. 1 (color online). Numerical measurement of creep compliance $J(s)$ in damped random spring networks for varying distance to isostaticity $\Delta z \equiv z - z_c$. For long time (low s), networks below isostaticity begin to flow [$J \sim 1/s$ (dashed line)], while networks above isostaticity achieve a finite strain.

affine velocity $\dot{\vec{U}}^{\mathrm{aff}} = \dot{\gamma}\vec{X}$ at its position $\vec{X}$, which is also the mean velocity $\langle\dot{\vec{U}}(\vec{X})\rangle$. Nonaffine damping is widely employed in studies of slow flows of foams, emulsions, and dense suspensions [23–26] and can be motivated in two ways: first, as an approximate Stokes drag that neglects any hydrodynamic interactions between nodes intermediated by a background fluid or, second, as a mean field approximation for relative damping between connected nodes. We set the stiffness k, the damping b, and the mean spring length all to unity. Equations of motion and numerical details are in the Supplemental Material [27].

Gradients in the solid and fluid phases.—Quasistatic ($\omega = 0$) shear stretches and compresses springs in a solid. The normal motion $u_{ij}^{\parallel}$ in spring (ij) is a discrete gradient of the displacement field $\vec{U}$ along $\hat{n}$, which varies from spring to spring. We assume this gradient is dominated by $\vec{U}^{\mathrm{na}}$. For scaling purposes, we introduce an unspecified quantity λ_s that relates the typical value of $u^{\parallel}$ and the typical nonaffine motion U^{na}:

$$u^{\parallel} \sim \frac{U^{\mathrm{na}}}{\lambda_s}. \tag{1}$$

A similar relation is found in the trial modes used to describe vibrational modes of marginal solids in Ref. [18], which are formed from floppy modes modulated by a sinusoidal envelope. Because $u^{\parallel}$ and U^{na} are related by a discrete gradient, we shall refer to λ_s as a length scale characterizing the solid (nonfloppy) phase.

Floppy modes permit a fluid to undergo zero frequency deformations without stretching springs. There can be nonaffine motion while $u^{\parallel}$ is everywhere zero, so Eq. (1) cannot describe a fluid. Instead, elastic forces in a fluid are induced by flow. At finite frequency ω (or finite rate s), nodes have finite velocity and experience viscous forces $\{\vec{F}_i\}$. Inertia is negligible at low frequencies, so these viscous forces must be balanced by elastic forces $\{\vec{f}_{ij}\}$ in the springs. The force balance equations $\sum_j \vec{f}_{ij} = \vec{F}_i$ are a discrete counterpart of the continuum relation div $\hat{\sigma} = \vec{\mathcal{F}}$, where $\vec{\mathcal{F}}$ is the viscous force density and the stress tensor $\hat{\sigma}$ is linear in the elastic forces. Thus viscous forces are related to gradients in the elastic forces, and, as above, we introduce an undetermined length scale λ_f relating the typical elastic force f and viscous force F in the fluid (floppy) phase:

$$F \sim \frac{f}{\lambda_f} \tag{2}$$

or, equivalently, $u^{\parallel} \sim \omega\lambda_f U^{\mathrm{na}}$. We will argue below that λ_s and λ_f are related to $\xi_\pm$.

In the following, an important consideration will be the complex shear modulus $G^*(\omega) = 1/J(s)|_{s=\imath\omega} \equiv G'(\omega) + \imath G''(\omega)$. Its real and imaginary parts G' and G'', the storage and loss moduli, are energy densities associated with elastic storage and viscous dissipation, respectively. The energy stored in springs scales as

$$G' \sim \vec{f}\cdot\vec{u} \sim \begin{cases} (\lambda_f U^{\mathrm{na}})^2\omega^2 & \text{with floppy modes} \\ (U^{\mathrm{na}}/\lambda_s)^2 & \text{without floppy modes,} \end{cases} \tag{3}$$

while dissipation by nonaffine damping scales as

$$G'' \sim \vec{F}\cdot\vec{U} \sim (U^{\mathrm{na}})^2\omega \tag{4}$$

both with and without floppy modes. Because $G^*(\omega)$ and $J(s)$ are related, for scaling purposes the inverse time scales ω and s are interchangeable.

Generalized isostatic length scale.—We first describe how to construct the diverging length scale $\xi_\pm(\Delta z, \omega)$ before relating it to $\lambda_{s,f}$. The subscript indicates the sign of Δz. In the standard scaling scenario near a critical point [16], the diverging length scale displays three qualitatively distinct regimes [Figs. 2(a) and 2(b)]. Two persist at zero frequency and can be probed by approaching z_c from above and below at $\omega = 0$. The third regime is inherently dynamical and can be probed by approaching z_c along the frequency axis.

Our approach generalizes the *cutting argument* of Refs. [17,18], which constructs the isostatic length scale $\ell^* \sim 1/\Delta z$. Thus by definition, ξ_+ will recover ℓ^* in the quasistatic limit. We first reprise the cutting argument by approaching z_c from above at $\omega = 0$.

On long enough wavelengths it is reasonable to approximate a material as a continuum; ℓ^* is the length scale beyond which this approximation is valid. One way to identify ℓ^* is to consider the properties of a finite portion

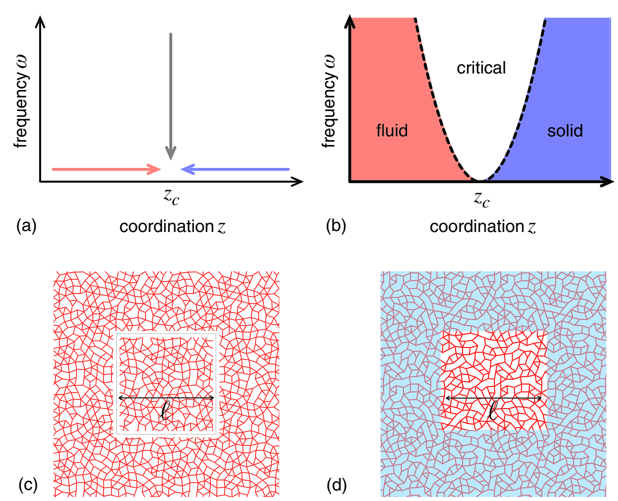

FIG. 2 (color online). (a) Three approaches to the critical point: along the z axis from above and below and along the frequency axis. (b) The length scale $\xi_\pm$ has three regimes, distinguished by comparing the frequency ω to the diverging time scale $\tau^* \sim 1/\Delta z^2$ (dashed curve). (c) *Cutting out* a subsystem of size ℓ. Springs crossing the dashed line are removed. (d) Creating a finite system by *freezing*. Nodes in the shaded region are not allowed to move.

of the infinite system. A sample with linear size ℓ that has the same properties as the infinite system is larger than ℓ^*, while a qualitatively different sample—e.g., one that no longer resists quasistatic shear—is smaller than ℓ^*.

So motivated, we imagine *cutting out* a sample of an infinite random spring network with excess coordination Δz. To do this, we overlay a box of size ℓ on the infinite system and cut those springs that cross its boundary; see Fig. 2(c). Cutting springs is destabilizing: Cut enough and floppy modes will appear. When this happens, the finite system must respond qualitatively differently to driving, as it cannot resist zero frequency shear: ℓ^* is the size of the box for which the first floppy mode appears. This occurs when the number of cut springs, proportional to the surface area ℓ^{d-1}, exceeds the number of excess contacts, which is proportional to $\Delta z \ell^d$. Hence $(\ell^*)^{d-1} \sim \Delta z (\ell^*)^d$, or $\xi_+(\Delta z, 0) \equiv \ell^* \sim 1/\Delta z$.

We now approach z_c from below. Clearly, repeating the cutting approach will not work in a system that already has floppy modes. As cutting is in essence the introduction of a free boundary, we now, instead, introduce a rigid boundary by *freezing* the position of nodes exterior to a box of linear size ℓ [see Fig. 2(d)]. Freezing introduces stability: Springs constrain floppy motion, and, while each spring in the bulk is shared by two nodes, those springs connected at one end to a frozen node are not shared. Hence there are more constraints per degree of freedom in the finite system, and by choosing ℓ small enough we can remove all of its floppy modes. The counting is entirely analogous to the surface area-to-volume ratio described above and gives $\xi_-(\Delta z, 0) \sim 1/(-\Delta z)$, the size of a finite sample with one floppy mode.

Last, we approach z_c along the frequency axis. Recall that for the quasistatic systems, $\xi_\pm(\Delta z, 0)$ is the length scale for which a rigid system becomes floppy, or vice versa, under the influence of a boundary. As deformations of random spring networks at finite frequency both store and dissipate energy, to proceed in analogy to the quasistatic case we should ask for what length scale storage and dissipation are comparable. A length scale can be imposed by either cutting or freezing. In both cases we will assume that the effect of the boundary is to impose the gradient lengths, i.e., $\lambda_s \simeq \ell$ and $\lambda_f \simeq \ell$.

Let us first impose a boundary by freezing. The finite system has no floppy modes, so low frequency storage will dominate loss. By Eqs. (3) and (4), the ratio of loss to storage is $G''/G' \sim \ell^2 \omega$, which is of the order of unity when $\ell = \xi_-(0, \omega) \sim 1/\omega^{1/2}$. We identify this length scale with ξ_- because it was reached via freezing. If we instead create a finite system by cutting, loss dominates storage and $G''/G' \sim 1/\ell^2 \omega$, which is again of the order of unity when $\ell = \xi_+(0, \omega) \sim 1/\omega^{1/2}$.

In summary, we have used cutting and freezing arguments to infer a dynamic critical length scale $\xi_\pm(\Delta z, \omega)$. The length scale has two branches: a solid branch for $\Delta z > 0$ and a fluid branch for $\Delta z < 0$, which together can be expressed succinctly as

$$\xi_\pm(\Delta z, \omega) \sim \begin{cases} \pm 1/\Delta z & \omega\tau^* \ll 1 \\ 1/\omega^{1/2} & \omega\tau^* \gg 1. \end{cases} \tag{5}$$

The crossover is controlled by the diverging time scale $\tau^* \sim 1/\Delta z^2$, which follows from balancing the scaling of $\xi_\pm$ in different regimes. Because both branches of $\xi_\pm$ scale as $1/\omega^{1/2}$ near z_c, we can speak meaningfully of a single dynamic critical regime; see Fig. 2(b). $\xi_\pm$ is frequency-independent outside the critical regime.

One might expect that a diverging length scale can be measured from the two-point correlation function of U^{na}. However, as previously noted [28,29], the only length scale to emerge from nonaffine correlations is the system size L. In fact, ℓ^* has never been identified in a two-point correlation function, only via less direct methods [19–21]. Instead we probe $\lambda_s \propto [\langle (u_{ij}^{\parallel})^2 \rangle / \langle (U_i^{\mathrm{na}})^2 \rangle]^{1/2}$ and $\lambda_f \propto (\langle f_{ij}^2 \rangle / \langle F_i^2 \rangle)^{1/2}$ in periodic networks (no cutting or freezing), where $\langle \cdot \rangle$ refers to an average over springs or nodes, as appropriate. Results are plotted in Fig. 3(a). By rescaling λ_s and λ_f with Δz^a and the frequency with Δz^{-b} and varying a and b, we find data collapse for $a = 1.1(1)$ and $b = 2.1(1)$. Though indirect, this numerical evidence strongly suggests that λ_s and λ_f can be identified with ξ_+ and ξ_-, respectively. In the following, we take this identification as an ansatz.

Relating $\xi_\pm$ to response.—Given $\lambda_{s,f} \propto \xi_\pm$, Eqs. (3) and (4) relate the complex shear modulus to the typical magnitude of nonaffine motion U^{na}, which remains to be determined. As nonaffinity is a form of fluctuation, we expect it will diverge on approach to the critical point [16], $U^{\mathrm{na}} \sim \xi_\pm^\nu$ for some $\nu > 0$. Its value $\nu = 1/2$ was previously derived for quasistatic hyperstatic networks [5]. In hypostatic networks, ν can be determined from the divergence of the dynamic (zero frequency) viscosity $\eta_0 \sim 1/(-\Delta z)$ (see Supplemental Material [27]). The viscosity diverges because low frequency motions of hypostatic networks strongly project on their floppy modes; η_0^{-1} is controlled by the floppy mode number density, which is proportional to $z_c - z$. Recalling that $\eta_0 = \lim_{\omega \to 0} G''/\omega$ and comparing to Eq. (4), we conclude that $\nu = 1/2$ on either side of z_c, as confirmed in the inset in Fig. 3(a).

With an expression for the gradient length scales and the value of ν, we have predictions for the scaling of G' and G''. These can be expressed compactly by introducing shear moduli $G_\pm \sim 1/\xi_\pm$ and viscosities $\eta_\pm \sim \xi_\pm$. For hyperstatic networks, Eqs. (3) and (4) become

$$G' \sim G_+ \quad \text{and} \quad G'' \sim \eta_+ \omega. \tag{6}$$

Appealingly, this is the complex shear modulus of the Kelvin-Voigt solid, i.e., elastic and viscous elements with coefficients G_+ and η_+ connected in parallel. Similarly,

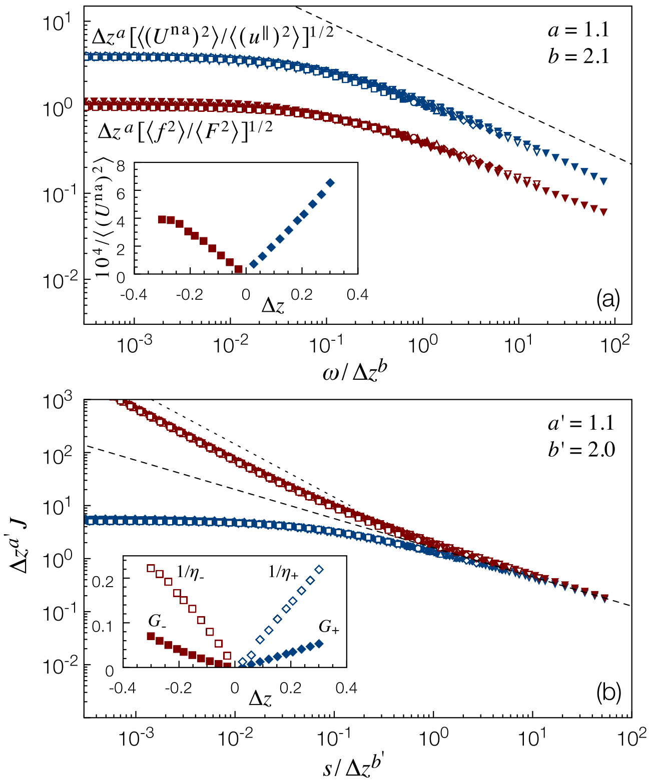

FIG. 3 (color online). Scaling collapse of data from simulated networks. The legend is as in Fig. 1. (a) The length scales $\lambda_{s,f}$ determined from the response to shear at frequency ω. The dashed curve has slope $-a/b$. Inset: $1/(U^{na})^2$ vanishes linearly at z_c in the zero frequency limit. (b) Scaling collapse of the compliance data in Fig. 1. The short and long dashed curves have slopes -1 and $-a'/b'$, respectively. Inset: Elastic and viscous coefficients in the zero frequency limit.

for hypostatic systems we recover the low frequency moduli of elements G_- and η_- connected in series, i.e., a Maxwell fluid,

$$G' \sim (\eta_-\omega)^2/G_- \quad \text{and} \quad G'' \sim \eta_-\omega. \tag{7}$$

Thus a network's complex shear modulus is always described by an elastic element $G_\pm$ and a viscous dashpot $\eta_\pm$. Above isostaticity, they are wired as a solid; below isostaticity, they are wired as a fluid.

Numerical results.—We provide two numerical tests of Eqs. (6) and (7). The first probes the quasistatic limit and confirms the scaling of $G_\pm$, which is given by $\lim_{\omega\to 0} G'$ above z_c and $\lim_{\omega\to 0}(G'')^2/G'$ below, and $\eta_\pm = \lim_{\omega\to 0} G''/\omega$. Figure 3(b) (inset) shows that, as predicted, both $G_\pm$ and $1/\eta_\pm$ grow linearly with Δz on either side of z_c.

Our second test revisits the compliance data of Fig. 1; by collapsing $J(s)$, we verify the finite rate dependence of $\xi_\pm \sim 1/s^{1/2}$. In hyperstatic networks the compliance is dominated by storage, $J \sim 1/G_+ \sim \xi_+(\Delta z, s)$, while in hypostatic systems it is controlled by loss, $J \sim 1/\eta_- s \sim 1/[\xi_-(\Delta z, s)s]$. Therefore, plotting $\Delta z^{a'} J$ versus $s/\Delta z^{b'}$ for $a' = 1$ and $b' = 2$ should collapse data from all three regimes of Fig. 2(b) to a two-branched master curve. Indeed, we find excellent collapse for $a' = 1.1(1)$ and $b' = 2.0(1)$ [Fig. 3(b)]. In the critical regime the compliance $J \sim 1/s^{1/2}$: Strain grows anomalously with the square root of time. This is reminiscent of Andrade creep in metals, although the Andrade exponent is $1/3$ [30].

Conclusions.—We have demonstrated dynamic critical scaling in damped, nearly isostatic spring networks and related the scaling to a diverging length scale $\xi_\pm$. At frequencies low compared to $1/\tau^*$, $\xi_\pm$ is controlled by the distance to isostaticity, networks behave as simple viscoelastic solids or fluids, and their elastic and viscous moduli are set by Δz. At higher frequencies, $\xi_\pm$ is determined by the rate at which the system is driven, storage and loss are comparable, and the distinction between solid and fluid is blurred.

Wyart and co-workers have shown that floppy motions in hypostatic networks are exponentially localized on a new length l_c that scales as $1/\Delta z^{1/2}$ at zero frequency and $1/\omega^{1/4}$ above $1/\tau^*$ [12,13]. Any quantity that scales with ξ_- will also scale with l_c^2, so scaling collapse such as in Fig. 3 cannot distinguish between them. On the other hand, there is strong theoretical and numerical evidence that quasistatic response in hyperstatic systems, including U^{na} [5], the quasistatic shear modulus G_0 [9,15], and point force response [20], is governed by ℓ^*, the quasistatic limit of ξ_+. It would be surprising if different length scales govern response above and below z_c.

Though we have treated spring networks, our predictions, in particular the rate dependence of the compliance and shear modulus, match prior results for G^* in jammed solids [9] and biopolymer networks [10] and the relaxation modulus in athermal suspensions [7]. This suggests the broader applicability of the scaling arguments presented here, which we expect can be extended to incorporate additional physics, including bending stiffness [4,11], finite strain amplitude [5,14,31], and steady flow [32].

This work was supported by the Dutch Organization for Scientific Research (NWO).

[1] J. Maxwell, Philos. Mag. **27**, 294 (1864).
[2] S. Alexander, Phys. Rep. **296**, 65 (1998).
[3] M. Thorpe, D. Jacobs, M. Chubynsky, and J. Phillips, J. Non-Cryst. Solids **266–269**, 859 (2000).
[4] C. Heussinger and E. Frey, Phys. Rev. Lett. **96**, 017802 (2006).
[5] M. Wyart, H. Liang, A. Kabla, and L. Mahadevan, Phys. Rev. Lett. **101**, 215501 (2008).
[6] W. G. Ellenbroek, Z. Zeravcic, W. van Saarloos, and M. van Hecke, Europhys. Lett. **87**, 34 004 (2009).
[7] T. Hatano, Phys. Rev. E **79**, 050301 (2009).

[8] M. van Hecke, J. Phys. Condens. Matter **22**, 033 101 (2010).
[9] B. P. Tighe, Phys. Rev. Lett. **107**, 158303 (2011).
[10] C. P. Broedersz, M. Depken, N. Y. Yao, M. R. Pollak, D. A. Weitz, and F. C. MacKintosh, Phys. Rev. Lett. **105**, 238101 (2010).
[11] C. P. Broedersz, X. Mao, T. C. Lubensky, and F. C. MacKintosh, Nat. Phys. **7**, 983 (2011).
[12] M. Wyart, Europhys. Lett. **89**, 64 001 (2010).
[13] G. Düring, E. Lerner, and M. Wyart, arXiv:1204.3542v1.
[14] M. Sheinman, C. P. Broedersz, and F. C. MacKintosh, Phys. Rev. E **85**, 021801 (2012).
[15] B. P. Tighe, arXiv:1205.2960v1.
[16] B. I. Halperin and P. C. Hohenberg, Phys. Rev. **177**, 952 (1969).
[17] A. V. Tkachenko and T. A. Witten, Phys. Rev. E **60**, 687 (1999).
[18] M. Wyart, S. R. Nagel, and T. A. Witten, Europhys. Lett. **72**, 486 (2005).
[19] L. E. Silbert, A. J. Liu, and S. R. Nagel, Phys. Rev. Lett. **95**, 098301 (2005).
[20] W. G. Ellenbroek, E. Somfai, M. van Hecke, and W. van Saarloos, Phys. Rev. Lett. **97**, 258001 (2006).
[21] M. Mailman and B. Chakraborty, J. Stat. Mech. (2011) L07 002.
[22] D. J. Jacobs and M. F. Thorpe, Phys. Rev. E **53**, 3682 (1996).
[23] D. J. Durian, Phys. Rev. Lett. **75**, 4780 (1995).
[24] P. Olsson and S. Teitel, Phys. Rev. Lett. **99**, 178001 (2007).
[25] E. Lerner, G. Düring, and M. Wyart, Proc. Natl. Acad. Sci. U.S.A. **109**, 4798 (2012).
[26] B. Andreotti, J.-L. Barrat, and C. Heussinger, Phys. Rev. Lett. **109**, 105901 (2012).
[27] See Supplemental Material at http://link.aps.org/supplemental/10.1103/PhysRevLett.109.168303 for equations of motion and a calculation of the dynamic viscosity in hypostatic networks.
[28] B. A. DiDonna and T. C. Lubensky, Phys. Rev. E **72**, 066619 (2005).
[29] C. E. Maloney, Phys. Rev. Lett. **97**, 035503 (2006).
[30] M.-C. Miguel, A. Vespignani, M. Zaiser, and S. Zapperi, Phys. Rev. Lett. **89**, 165501 (2002).
[31] B. P. Tighe and J. E. S. Socolar, Phys. Rev. E **77**, 031303 (2008).
[32] B. P. Tighe, E. Woldhuis, J. J. C. Remmers, W. van Saarloos, and M. van Hecke, Phys. Rev. Lett. **105**, 088303 (2010).